Geophys. J. Int. (1994) **117**, 257–264

Magnetic enhancement and palaeoclimate: study of a loess/palaeosol couplet across the Loess Plateau of China

M. E. Evans[1] and F. Heller[2]

[1] *Institute of Geophysics, Meteorology and Space Physics, University of Alberta, Edmonton,* T6G 2J1 *Canada*
[2] *Institut für Geophysik, ETH-Hönggerberg,* CH-8093 *Zürich, Switzerland*

Accepted 1993 September 6. Received 1993 September 3; in original form 1993 July 1

SUMMARY

The origin of the Milankovitch palaeoclimatic signal so dramatically recorded in the Chinese loess remains uncertain. At least five hypotheses have been put forward to explain the well-documented enhancement of magnetic susceptibility in palaeosols which formed when conditions were warmer and wetter. We report here a magnetic study of a prominent loess–soil couplet (L4-S3) at three widely separated sites where present-day mean annual rainfall and temperature range from ~350 mm to ~700 mm and from ~6 °C to ~13 °C. The properties determined are laboratory remanences (isothermal, IRM; anhysteretic, ARM; viscous, VRM, including viscous decay), room-temperature susceptibility, and thermomagnetic behaviour. At fields beyond 100 mT, the IRM spectra are all essentially identical, both in shape and in absolute magnitude, suggesting a uniform magnetic component widespread across the Plateau. Subtracting the signal of this component isolates a second component, the amount of which varies by an order of magnitude between sites. The magnetic properties of this latter material are remarkably similar to those reported for bacterial magnetite in geological sediments and modern soils. Viscous decay of VRM takes place in two distinct stages, one of which falls to zero in <10 min. We attribute magnetic enhancement—which is the source of the palaeoclimatic signal—to *in situ* pedogenetic formation of magnetite, which we characterize in our interpretation as two separate forms of bacterial magnetofossils. The most magnetic sample requires a mass fraction of about half of one per cent of this biogenic material.

Key words: bacterial magnetite, loess, magnetic susceptibility, palaeoclimate, palaeosol.

Downloaded from https://academic.oup.com/gji/article/117/1/257/616632 by guest on 16 August 2022

INTRODUCTION

The loess deposits that blanket large areas in China are known to carry significant palaeomagnetic and palaeoclimatic records (Heller & Liu 1982). In the former, magnetic remanence delineates the pattern of reversals and hence provides a means of correlating to the geomagnetic polarity chrons. In the latter, magnetic susceptibility acts as a climatic proxy and hence provides a means of correlating to the oxygen isotope stages (e.g. Imbrie *et al.* 1984). Despite their importance, however, the origin of both signals remains uncertain. Here, we consider the mineral magnetic basis of the palaeoclimatic signal.

Macroscopically, climatic oscillations manifest themselves in terms of alternations of loess and palaeosols, unaltered loess corresponding to cold, arid conditions (glacials), palaeosols reflecting warmer, wetter times (interglacials and interstadials). At three sites (Baicoayuan, Luochuan and Baoji), we have investigated samples from a prominent palaeosol (S3) and the underlying loess (L4) from which it developed. The sites are indicated on Fig. 1, together with susceptibility profiles from the surface down to the base of L4. Peaks associated with S1, S2 and S3 correspond to oxygen isotope stages 5, 7 and 9, respectively. By examining three sites separated by hundreds of kilometres we sought to identify any commonality, but also to discern the influence of local climatic conditions on the degree of pedogenesis and the evolution of magnetic minerals. At the present time the mean annual temperature and rainfall are ~6 °C and ~350 mm at Baicaoyuan, ~9 °C and ~620 mm at Luochuan, and ~13 °C and ~700 mm at Baoji.

A uniform series of measurements was carried out on

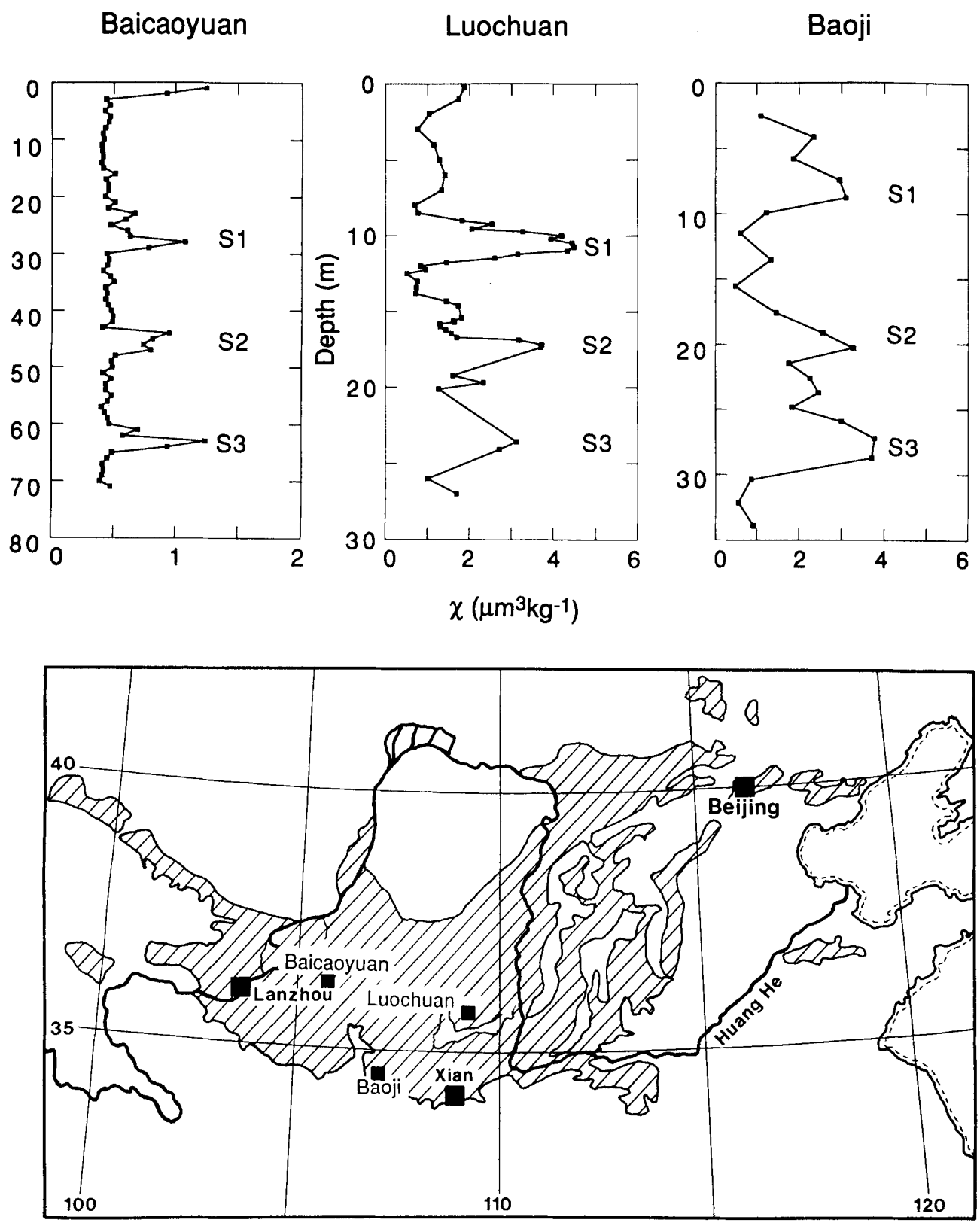

Figure 1. Sketch map showing the three sites studied (small squares) and corresponding susceptibility profiles down to the base of L4. The geographical extent of loess is indicated by shading.

Downloaded from https://academic.oup.com/gji/article/117/1/257/616632 by guest on 16 August 2022

representative samples from each site: room-temperature low-field susceptibility (χ, both high and low frequency), acquisition of viscous remanence (VRM) followed by monitoring of the viscous decay, incremental acquisition of anhysteretic remanence (ARM) followed by progressive alternating field (AF) demagnetization, and incremental acquisition of isothermal remanence (IRM) followed by progressive demagnetization (both AF and direct 'back' field). In addition, thermomagnetic (Curie balance) curves were determined on parallel samples consisting of disaggregated powders.

EXPERIMENTAL RESULTS

Isothermal remanent magnetization

Acquisition of IRM was monitored at 20 steps in steadily increasing fields up to a maximum of 900 mT. Compared to the parent L4 material, the S3 samples are more magnetic, but have lower coercivities (Fig. 2a). The IRM S3/L4 ratios at 900 mT are 1.3, 2.4 and 3.0 at Baicaoyuan, Luochuan and Baoji, respectively; corresponding S3/L4 median acquisition fields are 60/80 mT, 32/68 mT, and 27/60 mT. Above 100 mT, the curves are all essentially coincident, with partial IRMs (>100 mT) always close to 2 $mAm^2 kg^{-1}$ (Fig. 2b). We interpret this in terms of a two-component system; an underlying population of magnetic particles (component A) which is essentially uniform across the loess plateau, with a superimposed population (component B) that varies in magnitude from site to site.

To assess this model more fully, it is necessary to know the complete coercivity spectrum of component A, not just the part >100 mT. For this purpose, we take the L4 sample from Baicaoyuan (BY52) to be representative. It is from the most arid of the three sites, and is therefore least likely to have been affected by weathering, but the strongest reasons for this choice are based on the susceptibility and VRM data, as will be seen presently. We proceed by subtracting the BY52 curve from each of the others. The difference curves obtained for each of the S3 samples are given in Fig. 2(c). In absolute units, the soil at Baicaoyuan has a B component with a saturation IRM (SIRM) of 1.46 $mAm^2 kg^{-1}$, corresponding SIRMs at Luochuan and Baoji being five and 10 times this, respectively (Table 1). Despite this order of magnitude range in absolute terms, the individual spectra all have identical shapes, as shown by the normalized curves in Fig. 2(d). The component B median acquisition field MAF, sometimes referred to as the remanent acquisition coercive force, B'_{cr} (Dankers 1981) is 21 mT, compared to 80 mT for component A (sample BY52).

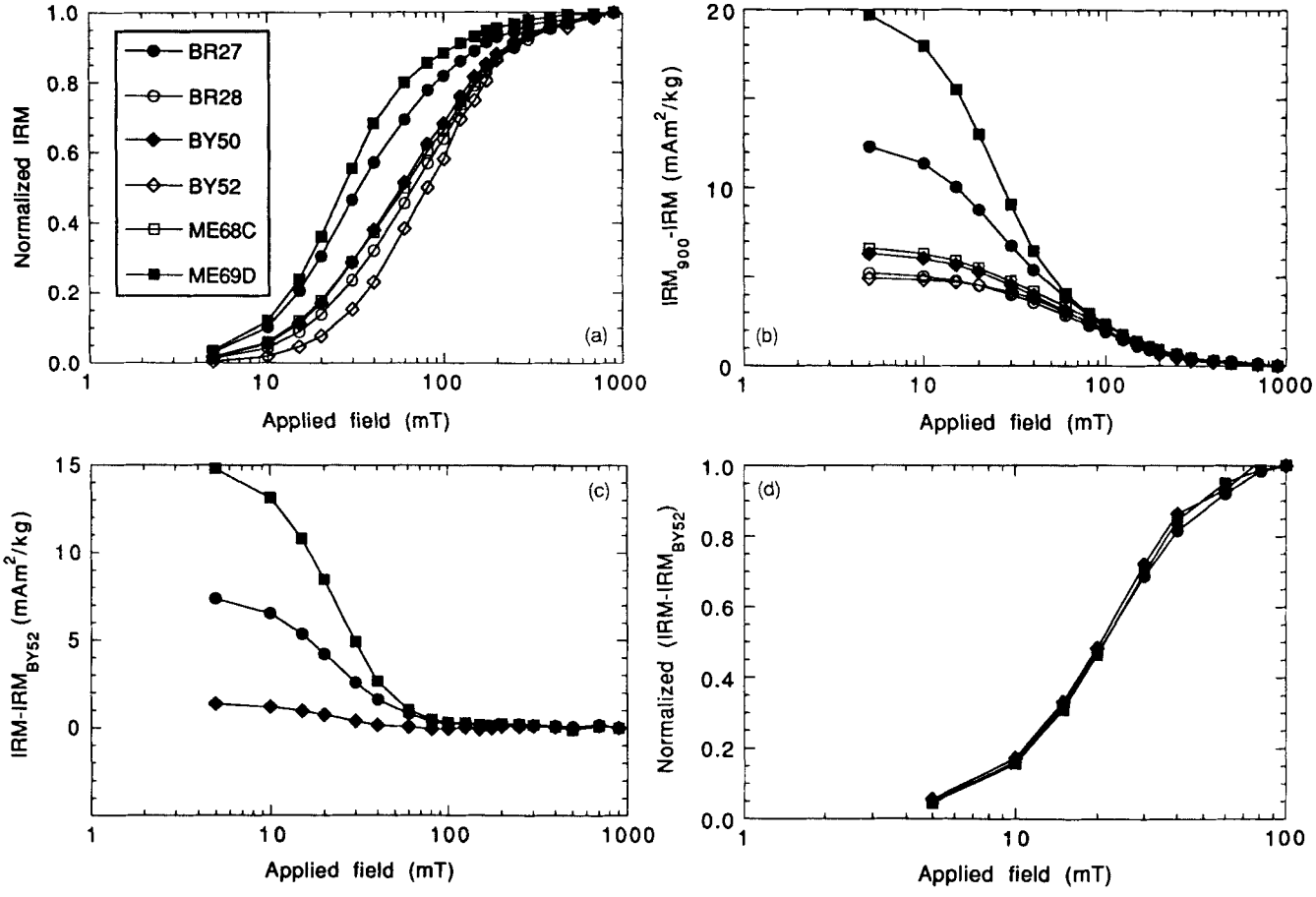

Figure 2. Acquisition of IRM. (a) Normalized cumulative curves. Symbols are retained throughout the paper (diamonds = Baicaoyuan; circles = Luochuan; squares = Baoji: solid = S3; open = L4). (b) $IRM_{900\,mT}$–IRM. (c) $IRM–IRM_{BY52}$ (= component B). (d) Normalized cumulative curves for component B.

Downloaded from https://academic.oup.com/gji/article/117/1/257/616632 by guest on 16 August 2022

Table 1. Summary of magnetic properties.

	BY50 S3	BY52 L4	BR27 S3	BR28 L4	ME69 S3	ME68 L4
IRM (mAm^2/kg)	6.40	4.94	12.7	5.27	20.4	6.69
ARM (mAm^2/kg)	0.404	0.139	1.22	0.242	2.37	0.447
χ ($\mu m^3/kg$)	0.645	0.293	1.97	0.416	3.42	0.667
T_C (°C)	587	572	578	568	577	581
B'_{cr} (mT)	60	80	32	68	27	60
MDF_{IRM} (mT)	24	31	17	27	16	26
B_{cr} (mT)	38	51	23	42	22	40
MDF_{ARM} (mT)	26	56	20	31	20	27
χ_{ARM} ($\mu m^3/kg$)	5.08	1.74	15.4	3.03	29.8	5.61
F (%)	8.10	1.80	10.8	4.30	11.3	8.20
VRM ($\mu Am^2/kg$)	3.13	---	9.20	1.34	16.7	3.74
S_I ($\mu Am^2/kg$)	0.870	---	4.55	0.381	6.07	1.24
S_{II} ($\mu Am^2/kg$)	0.750	---	1.91	0.327	4.03	0.751

Note: IRM acquired in 900 mT. ARM acquired in 200 mT. χ measured at 0.47 kHz. VRM from 30 s to 10 000 s. S regression lines have $R \geq 0.9985$.

The 900 mT IRMs were incrementally demagnetized in 13 steps up to a maximum peak alternating field of 100 mT, and the results analysed in the same way as the acquisition curves. After normalization, the three soils are again virtually identical (Fig. 3), with a B component median destructive field (MDF) of 14 mT. By contrast, component A has an MDF of 31 mT.

After AF demagnetization, the samples were remagnetized in a steady field of 900 mT and then demagnetized by increasing reverse DC fields to determine the coercivity of remanence (B_{cr}). Again, the soils are systematically softer, with $22\,mT < B_{cr} < 38\,mT$, compared to 40–51 mT for the loess samples (Table 1). After subtraction of the component A contribution, the three soil curves are essentially coincident, with $B_{cr} = 18$ mT. As previously found by several investigators (Dankers 1981; Dunlop 1986; Maher 1988), there is support for the empirical observation that $MAF + MDF \approx 2B_{cr}$.

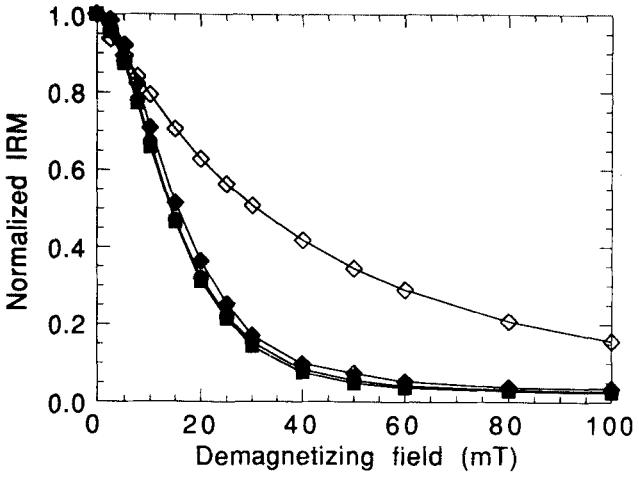

Figure 3. Progressive AF demagnetization of IRM of component B. The curve for BY52 (= component A) is shown for comparison.

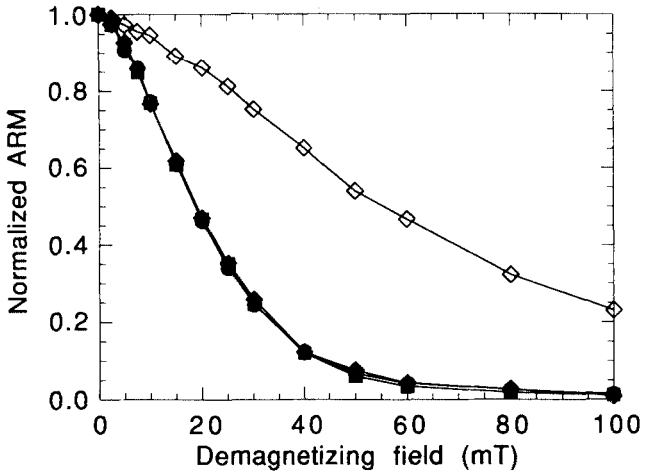

Figure 4. Progressive AF demagnetization of ARM of component B. The curve for BY52 (= component A) is shown for comparison.

Anhysteretic remanent magnetization

The samples were given anhysteretic remanences in a steady field of 0.1 mT with successive alternating fields of 40, 80, 120, 160 and 200 mT, followed by progressive AF demagnetization as for the IRM experiments. The overall pattern of behaviour is similar to the IRM data, except that intensities are about an order of magnitude lower (Table 1). The ARM S3/L4 ratios at 200 mT are 2.9, 5.0 and 5.3 at Baicaoyuan, Luochuan and Baoji, respectively. After subtracting the component A signal, the three palaeosol samples are indistinguishable from one another (Fig. 4). The MDF is 19 mT, compared to 56 mT for component A.

Room-temperature low-field susceptibility

Susceptibilities (χ) were measured at two frequencies (0.47 and 4.7 kHz) on a Bartington MS2 meter, and the results are summarized in Table 1. Low-frequency values range from 0.29 to 3.4 $\mu m^3 kg^{-1}$, and show the systematic difference between loess and soils expected from numerous earlier investigations. The χ S3/L4 ratios at Baicaoyuan, Luochuan and Baoji are 2.2, 4.7 and 5.1, respectively. High-frequency susceptibilities are usually expressed in terms of the so-called F-factor, which is the percentage loss in χ when measured at the higher frequency. At each of the three sites, F is higher in S3 than in the corresponding L4; as the loess is converted to soil, F increases from 1.8 per cent to 8.1 per cent at Baicaoyuan, from 4.3 per cent to 10.8 per cent at Luochuan, and from 8.2 per cent to 11.3 per cent at Baoji. The low values of χ and F for the L4 material at Baicaoyuan motivated us to use sample BY52 to model the ubiquitous magnetic phase (component A). This follows from the observation of Heller *et al.* (1991) that as loess transforms to soil, these parameters evolve in a distinctive way (Fig. 5). Samples plotting near the lower left represent the initial stages of the process, which Heller *et al.* refer to as the 'ground level'.

The F-factor itself is widely used to indicate the presence of ultrafine particles spanning the threshold between stable

Downloaded from https://academic.oup.com/gji/article/117/1/257/616632 by guest on 16 August 2022

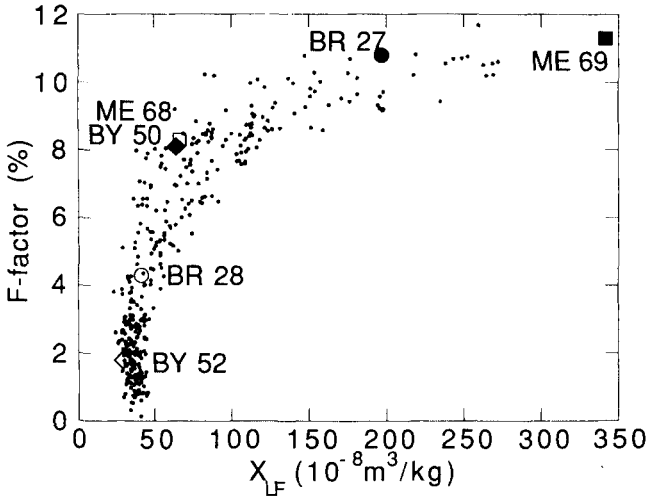

Figure 5. Room-temperature (low-field, low-frequency) susceptibility (χ) versus F-factor. The small dots represent corresponding data from 380 samples from the three sites studies.

single domain (SSD) and superparamagnetic (SP) behaviour. This follows from standard Néel theory (Stephenson 1971a); at a frequency of 470 Hz the susceptibility of a population of grains increases abruptly by a factor of 15 as they cross this boundary. The actual values of F provide qualitative, rather than quantitative, grain-size information. For a particular grain-size distribution (in which the number of grains within a given volume range is inversely proportional to the square of the volume), Stephenson (1971b) derives a theoretical value of 14 per cent per frequency decade. Our S3 F-factors (8–11 per cent) indicate that ultrafine grains are important, but they do not provide a direct quantitative measure. Furthermore, the L4 samples from Luochuan and Baoji also have enhanced F-factors (4 and 8 per cent, respectively). What, then, is the connection between susceptibility enhancement and the production of component B deduced from the remanence measurements? To a considerable degree, the two types of experiment are mutually exclusive because SP grains carry no remanence. The simplest hypothesis is that pristine loess material starts out with a population of magnetic grains (A), to which is added, *in situ*, varying amounts of a second population (B) which includes both SSD *and* SP grains; the SSD material accounts for the remanence, the SP for the susceptibility.

Thermomagnetic analysis

Disaggregated samples of S3 and L4 from the three sites were analysed thermomagnetically in a horizontal translation balance in which a heating rate of 12 °C min^{-1} was maintained. The results are illustrated in Fig. 6. In all cases, the heating curves are dominated by a mineral with a Curie point within 10° of 578 °C, as determined by the method of Moskowitz (1981) (Table 1). There can be little doubt that this is fairly pure magnetite. Near 300 °C the heating curves show an inflection—sometimes marked, sometimes subtle—which indicates the presence of significant amounts of maghemite. This mineral is thermally unstable and converts to haematite as heating progresses, leading to a decrease of magnetization on subsequent cooling by as much as 30 per cent. Beyond 600 °C the signals are all very weak compared to the sensitivity of the instrument, and it is not possible to discern any convincing signal from haematite, either newly created or originally present.

Magnetic viscosity

Samples were first AF demagnetized to 150 mT and then allowed to acquire VRMs by exposure to the laboratory

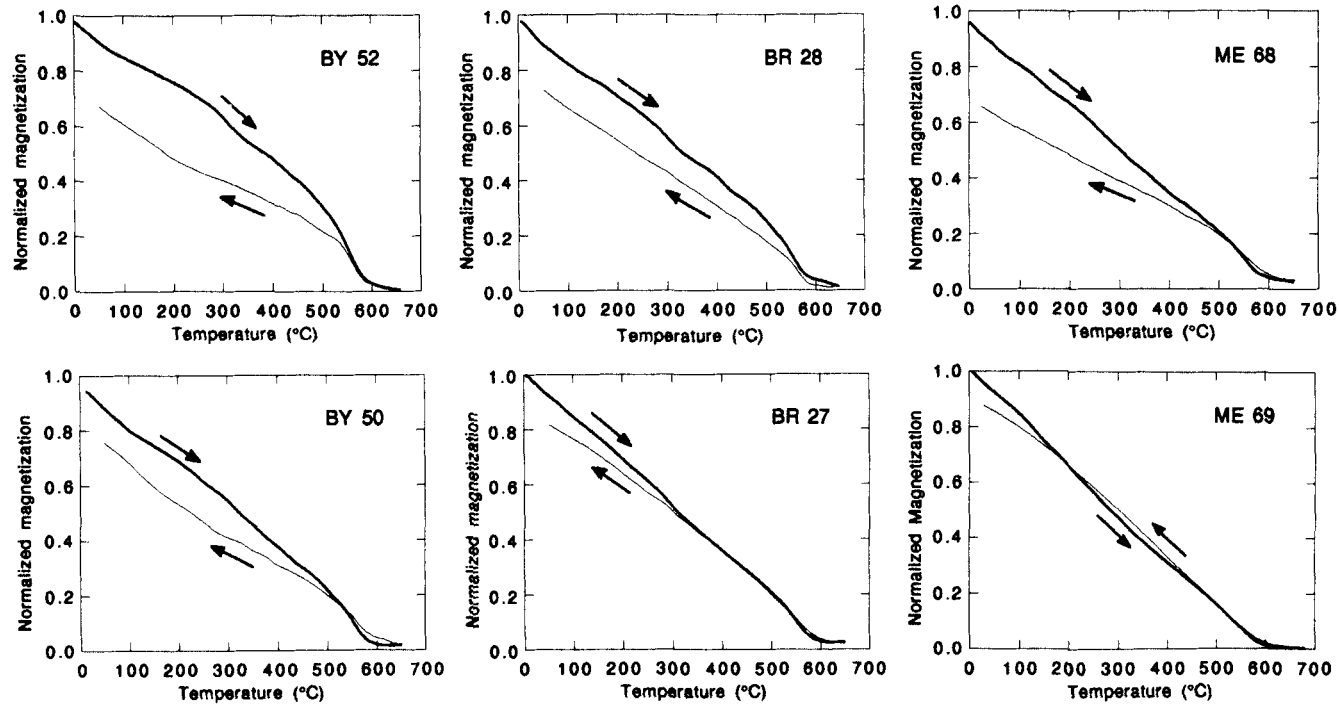

Figure 6. Thermomagnetic heating and cooling curves in air for disaggregated powders from the three sites studied. Applied field: 0.4 T.

Downloaded from https://academic.oup.com/gji/article/117/1/257/616632 by guest on 16 August 2022

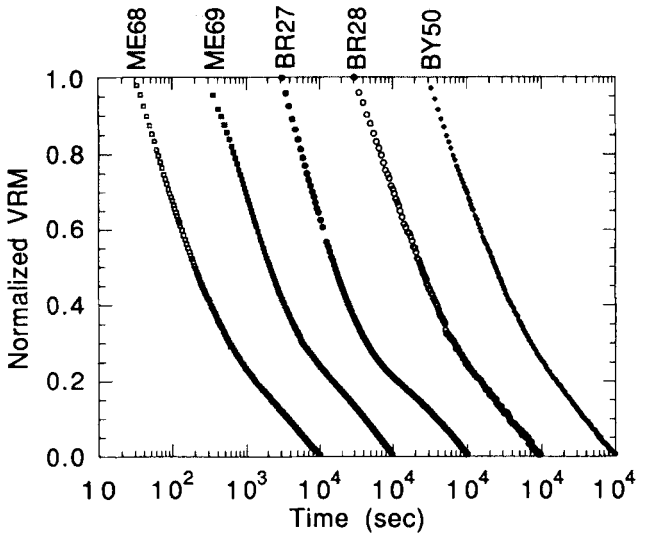

Figure 7. Viscous decay of VRM for elapsed time $t < 10\,000$ s, normalized to $t = 30$ s. The leftmost curve is correctly positioned; for clarity, the others are successively shifted by one decade.

geomagnetic field (47 μT) for several days. Viscous decay of the magnetizations so gained was monitored with a three-axis 2G cryogenic magnetometer for periods up to 14 hr. In the particular arrangement used, it is practically impossible to obtain the first reading before 20–30 s, so we normalized all the decay curves to an elapsed time of 30 s. At the other end of the decay process, beyond 5–6 hr, several of the VRMs had decayed to a level where the hard component not removed by the initializing AF demagnetization was no longer negligible. This manifests itself as a gradual change in direction of the total remanence vector and corresponding curvature of the decay curves. In order to have an unambiguous VRM signal, comparable from sample to sample, we restrict attention to elapsed times <3 hr, by which time 90 per cent, or more, of the decay ultimately recorded had taken place. The data for the interval 30 s to 3 hr are presented in Fig. 7. No result is given for sample BY52 since it acquired no measurable VRM; this is one of the main reasons for regarding it as original, unmodified, loess-containing component A but devoid of *in situ* (component B) magnetic enhancement.

The most striking feature is that all samples shown in Fig. 7 decay in two stages. For the purposes of discussion, we label these I and II. The stage I material is reduced to zero after 5–10 min, as indicated by the change in slope. Although the curves are all very similar when normalized in this way, it is important to realize that the starting (30 s) values range over a factor of 12.5 (Table 1). Viscous decay is usually characterized by a decay coefficient, S, where $\mathrm{VRM}(t)-\mathrm{VRM}(0) = S \log(t)$; two-stage decay therefore requires two coefficients S_{I} and S_{II}, the proper value of S_{I} being obtained by subtracting the underlying S_{II} from the observed slope during stage I. The two S values exhibit intersite patterns similar to the other parameters. For the soil samples, S_{I} ranges from 0.87 to 6.1 $\mu\mathrm{Am}^2\,\mathrm{kg}^{-1}$, S_{II} from 0.75 to 4.0 $\mu\mathrm{Am}^2\,\mathrm{kg}^{-1}$, as we pass from Baicaoyuan to Baoji.

DISCUSSION

First, we note that the Curie balance data indicate that fairly pure magnetite is an important constituent of all the samples investigated. There is evidence of significant amounts of maghemite, and there may well be other magnetic phases present (such as haematite) which are too weakly magnetic to be detected, but we agree with Maher & Thompson (1992) in recognizing the significance of the magnetitie contribution.

Laboratory remanences show marked intersite variations, the range of $\mathrm{IRM}_{900\,\mathrm{mT}}$ for S3 amounts to a factor of 3.2, while for L4 it is only 1.4. For $\mathrm{ARM}_{200\,\mathrm{mT}}$ the corresponding factors are 5.9 and 3.2, respectively. In other words, intersite variability in palaeosol is about twice what it is in loess, which suggests that the soil-forming process plays a significant role in determining the magnetic characteristics. More important, however, is the existence of a simple underlying pattern, despite the observed variability. Above 100 mT the IRM curves are virtually identical, leading to the concept of an underlying, pristine constituent (A), common to all three sites. This parallels the conclusions of Heller *et al.* (1991) involving a widespread bulk susceptibility minimum of about 40×10^{-5} (SI). The full collections available from the three sites studied in the present paper indicate similar minima, so that both susceptibility and remanence properties support the 'ground level' concept of Heller *et al.* (1991). Returning to the IRM curves, we note that at coercivities below 100 mT, order of magnitude differences take place across the plateau, which we attribute to varying amounts of a second constituent (B). While it may be possible to reconcile magnetization intensity differences up to a factor 10 with the 'constant influx/dilution' model of Kukla *et al.* (1988), it is more difficult to account for the pattern of coercivity spectra. These require that the soils not only become magnetically stronger, but that they also become magnetically softer. Rolph *et al.* (1993) argue that different source regions may control the magnetic properties of loess sequences in different parts of the plateau, but this is not favoured by the evidence from the three widely separated sites which we have investigated. The IRM spectra of the isolated B component (Fig. 8) suggest a population with a fixed

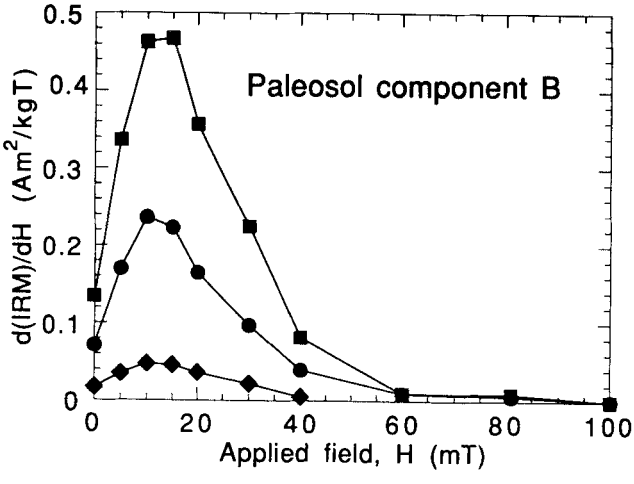

Figure 8. IRM spectra for component B.

Downloaded from https://academic.oup.com/gji/article/117/1/257/616632 by guest on 16 August 2022

coercivity signature which simply grows bigger towards the south and east. The simplest explanation is to attribute this to *in situ* pedogenic processes. This study, then, adds to the growing support for the importance of pedogenesis in understanding the magnetic recording of palaeoclimatic variations (Zhou *et al.* 1990; Heller *et al.* 1991; Maher & Thompson 1992; Banerjee, Hunt & Liu 1993).

Maher (1988) suggests a new scheme of magnetic granulometry in which the ratio ARM susceptibility (χ_{ARM})/SIRM is compared to the MDF of ARM. For the synthetic magnetites she studied, MDF_{ARM} ranges from 13 to 22 mT and the χ_{ARM}/SIRM ratio is generally in the range 1–2 mm A^{-1}. Large multidomained magnetites can have MDF_{ARM} values spanning this range, but the χ_{ARM}/SIRM ratios are always low (<0.2 mm A^{-1}). The two ends of a possible wide spread of grain sizes can therefore be discriminated. The B component in our S3 samples has $MDF_{ARM} = 19$ mT and χ_{ARM}/SIRM ratios in the range 1.8–2.3 mm A^{-1} suggesting that their magnetic properties are due to ultrafine magnetite grains with typical dimensions significantly less than 100 nm (Maher's samples have mean particle sizes ranging from 12 to 69 nm). A small spread of sizes will mean that both SSD and SP grains are present (Evans & McElhinny 1969; Butler & Banerjee 1975). The SSD grains will carry the remanence, the SP grains will dominate the susceptibility. Maher's data imply that the strongest of our samples (from Baoji) requires a magnetite fraction of only ~0.2 per cent for SIRM and ~0.4 per cent for χ, with the weakest (Baicaoyuan) needing one-tenth (SIRM) and one-fifth (χ) of these quantities.

There is a paucity of viscous decay data for sizes particles, but Dunlop (1983) obtains $S \approx 6$ mAm^2 kg^{-1} for a sample of synthetic magnetite particles averaging ~40 nm in size. This implies a total of ~0.3 per cent to explain the viscous behaviour of the Baoji sample. Agreement with the amount deduced from susceptibility is reasonable, bearing in mind that this kind of estimate provides only a rough guide. We can conclude that the most magnetic of our samples requires little more than half of one per cent of ultrafine magnetite particles to satisfactorily account for the measured magnetic properties of its component B.

Identical coercivity spectra found at all three sites for IRM and ARM suggest to us that the origin of these magnetite grains is bacterial. Petersen, van Dobeneck & Vali (1986) remark on the 'very high homogeneity' observed in the magnetic properties of a range of sediments in which they subsequently identified fossil magnetosomes. They draw attention to uniform MDF_{ARM} values of ~19 mT, and emphasize particular regions on diagnostic bi-parametric plots which typify this biogenic material: $12\text{ mT} < MDF_{IRM} < 15\text{ mT}$, $0.07 < (ARM/IRM) < 0.10$, and $4.5\text{ mT} < (MDF_{ARM} - MDF_{IRM}) < 7\text{ mT}$. For the *in situ* material in our S3 samples, we obtain $MDF_{ARM} = 19$ mT, $MDF_{IRM} = 14$ mT, $(ARM/IRM) = 0.08 \pm 0.01$, and $MDF_{ARM} - MDF_{IRM} = 5$ mT. The agreement is remarkable, but it must not be forgotten that Petersen *et al.* studied deep-sea sediments, not subaerial continental deposits. However, magnetotactic bacteria are known to occur in soil; in the example reported by Fassbinder, Stanjek & Vali (1990) they were found to contain 'unsubstituted pure magnetite' spanning the SSD/SP boundary, and amounting to ~0.035 wt per cent. Our S3 samples need up to ~17 times this, but given the ease with which environmental conditions influence bacterial population density (Vali *et al.* 1987), this is not a stumbling block. Inorganic magnetite can also form in soil (Maher & Taylor 1988), but it is difficult to see how this would give rise to identical populations across the Loess Plateau. Concerning the laboratory synthesis of submicron magnetite, Maher (1988) points out that different grain-size distributions were produced by 'slight modifications' of experimental procedure. A corresponding spread of magnetic properties results; for example, MDF_{ARM} ranges over almost a factor of three (10–29 mT). On the other hand, it is almost a requirement that uniformity should result from bacterial processes, since there are tight limits to the size of magnetic particles of use to a bacterium (Petersen *et al.* 1986). Biogenic magnetite of SSD size endows some advantage to the organism, and larger grains will be strongly selected against, whereas there is no reason why inorganic particles should avoid growing into the multidomain (MD) region. It is also noteworthy that Fassbinder *et al.* (1990; see also Petersen *et al.* 1993) find evidence of two types of bacterial magnetite, a generally larger set (40–100 nm) embedded within organic material or in the cell envelope, and a smaller set (20–40 nm) similar to the extracellular magnetite derived from GS-15 bacteria. The two-stage viscous decay that we observe is qualitatively consistent with these observations. We always find $S_I > S_{II}$ (by up to a factor of ~2), which could, of course, simply reflect greater amounts of S_I material. But excessive amounts are not required because there is a strong increase of S with decreasing grain size below about 60 nm (Dunlop 1983).

Our main aim has been to explore the way in which magnetic enhancement takes place as loess is transformed to soil, that is to consider the nature and origin of what we have called component B. However, we deduce the existence of a second, omnipresent component (A), the interpretation of which we now consider. It is characterized by coercivities extending at least as high as 900 mT, which indicates the presence of haematite. But component A cannot be exclusively composed of this mineral because the thermomagnetic data demonstrate the presence of magnetite and maghemite in sample BY52. Indeed, it is this sample in which the maghemite inflection near 300 °C and an unmistakable magnetite Curie point are most manifest. We conclude, therefore, that the original detrital input contained all three minerals. Approximate proportions can be estimated from the IRM curves by assuming that (1) all the remanence above 100 mT is due to haematite, and that this represents ~90 per cent of the haematite signal (haematite powders always have some coercivities <100 mT; see e.g. Dunlop 1972), and that (2) the abundance of maghemite relative to magnetite is given by the loss during heating in the Curie balance. From the BY52 data, (1) implies a haematite magnetization of ~2.2 mAm^2 kg^{-1}, leaving ~2.8 mAm^2 kg^{-1} to be attributed to the other two minerals, for which (2) implies a magnetite/maghemite split of ~70/30. Given intrinsic values (in Am^2 kg^{-1}) of 0.4, 70 and 92 for haematite, maghemite and magnetite respectively, and taking corresponding M_{rs}/M_s ratios of 0.5, 0.5 and 0.1 (O'Reilly 1984), we obtain mass fractions of 0.88 per cent, 0.024 per cent, and 0.022 per cent for the three constituents. These figures are approximate, but serve to indicate that an original magnetic input of about 1 per cent,

Downloaded from https://academic.oup.com/gji/article/117/1/257/616632 by guest on 16 August 2022

strongly dominated by haematite, suffices to explain the magnetic properties of pristine loess. These estimates are very close to those made by Maher & Thompson (1992) based on multiple regression of remanence and susceptibility data of 11 samples from four loess strata. They obtain 0.92 per cent for the haematite fraction and 0.05 per cent for magnetite. Their model—which is constrained at the outset—does not consider maghemite, which presumably gets combined with, and interpreted as, magnetite.

CONCLUSIONS

A series of mineral magnetic experiments has been carried out on samples from the L4/S3 couplet at three widely separated sites in the Loess plateau of north-central China. The main conclusions are:

(1) all samples possess an original airfall population of magnetic particles amounting to a mass fraction of about 1 per cent. This fraction is dominated by haematite, but also contains significant amounts of magnetite and maghemite. In L4, at least, it is remarkably uniform throughout the plateau.

(2) A second magnetic component consists of bacterial magnetite associated with pedogenesis. This component is very homogeneous as far as its magnetic characteristics are concerned, but it increases in amount by an order of magnitude from north-west (Baicaoyuan) to south-east (Baoji), where it comprises a mass fraction of about 0.5 per cent.

(3) Viscous decay always occurs in two stages, implying two subsets of magnetite particles, one of which decays to zero in 5–10 min. The emerging picture has much in common with the reported occurrence in modern soil of two types of bacterial magnetite, a larger (40–100 nm) intra cellular type, and a smaller (20–40 nm) extracellular type.

ACKNOWLEDGMENTS

Financial support was provided by the Natural Sciences and Engineering Research council of Canada and the Schweizerischer Nationalfonds zur Förderung der wissenschaftlichen Forschung, whilst M.E.E. was the recipient of an International Fellowship under the Canada/Switzerland bilateral exchange program. We are greatly indebted to many Chinese colleagues, particularly Ding Zhongli, who provided crucial guidance and sage advice.

REFERENCES

Banerjee, S.K., Hunt, C.P. & Liu, X.M., 1993. Separation of local signals from the regional paleomonsoon record of the Chinese loess plateau: A rock-magnetic approach, *Geophys. Res. Lett.*, **20,** 843–846.

Butler, R.F. & Banerjee, S.K., 1975. Theoretical single-domain grain size range in magnetite and titanomagnetite, *J. geophys. Res.*, **80,** 4049–4058.

Dankers, P., 1981. Relationship between median destructive field and remanent coercive forces for dispersed natural magnetite, titanomagnetite and hematite, *Geophys. J. R. astr. Soc.*, **64,** 447–461.

Dunlop, D.J., 1972. Magnetic mineralogy of unheated and heated red sediments by coercivity spectrum analysis, *Geophys. J. R. astr. Soc.*, **27,** 37–55.

Dunlop, D.J., 1983. Viscous magnetization of 0.04–100 μm magnetites, *Geophys. J. R. astr. Soc.*, **27,** 37–55.

Dunlop, D.J., 1986. Hysteresis properties of magnetite and their dependence on particle size: a test of pseudo-single-domain remanence models, *J. geophys. Res.*, **91,** 9569–9584.

Evans, M.E. & McElhinny, M.W., 1969. An investigation of the origin of stable remanence in magnetite-bearing igneous rocks, *J. Geomagn. Geoelectr.*, **21,** 757–773.

Fassbinder, J.W.E., Stanjek, H. & Vali, H., 1990. Occurrence of magnetic bacteria in soil, *Nature*, **343,** 161–163.

Heller, F. & Liu, T.S., 1982. Magnetostratigraphical dating of loess deposits in China, *Nature*, **300,** 431–433.

Heller, F., Liu, X.M., Liu, T.S. & Xu, T.C., 1991. Magnetic susceptibility of loess in China, *Earth planet. Sci. Lett.*, **103,** 301–310.

Imbrie, J., Hays, J.D., Martinson, D.G., Mcintyre, A., Mix, A.C., Morley, J.J., Pisias, N.G., Prell, W.L. & Shackleton, N.J., 1984. The orbital theory of Pleistocene climate: support from a revised chronology of the marine $\delta^{18}O$ record, in *Milankovitch and Climate*, Part I, pp. 269–305, eds Berger, A. *et al.*, Reidel, Dordrecht.

Kukla, G., Heller, F., Liu, X.M., Xu, T.C., Liu, T.S. & An, Z.S., 1988. Pleistocene climates in China dated by magnetic susceptibility, *Geology*, **16,** 811–814.

Maher, B.A., 1988. Magnetic properties of some synthetic sub-micron magnetites, *Geophys. J.*, **94,** 83–96.

Maher, B.A. & Taylor, R.M., 1988. Formation of ultrafine-grained magnetite in soils, *Nature*, **336,** 368–370.

Maher, B.A. & Thompson, R., 1992. Paleoclimatic significance of the mineral magnetic record of the Chinese loess and paleosols, *Q. Res.*, **37,** 155–170.

Moskowitz, B.M., 1981. Methods for estimating Curie temperatures of titanomaghemites from experimental J_s-T data, *Earth planet. Sci. Lett.*, **53,** 84–88.

O'Reilly, W., 1984. *Rock and Mineral Magnetism*, Blackie, Glasgow.

Petersen, N., von Dobeneck, T. & Vali, H., 1986. Fossil bacterial magnetite in deep-sea sediments from the South Atlantic Ocean, *Nature*, **320,** 611–615.

Petersen, N., Schmidbauer, E., Strattner, M. & Schüler, D., 1993. On the occurrence of bacterial magnetite in limnic sediments and soil, *Ann. Geophys.*, **11** (Suppl. 1), C90.

Rolph, T.C., Shaw, J., Derbyshire, E. & Wang, J.T., 1993. The magnetic mineralogy of a loess section near Lanzhou, China, in *The Dynamics and Environmental Context of Aeolian Sedimentary Systems*, ed. Pye, K., *Geol. Soc. Spec. Publ.*, **72,** 311–323.

Stephenson, A., 1971a. Single domain distributions. I. A. method for the determination of single domain grain distributions, *Phys. Earth planet. Inter.*, **4,** 353–360.

Stephenson, A., 1971b. Single domain distributions. II. The distribution of single domain iron grains in Apollo 11 lunar dust, *Phys. Earth planet. Inter.*, **4,** 361–369.

Vali, H., Förster, O., Amarantidis, G. & Petersen, N., 1987. Magnetotactic bacteria and their magnetofossils in sediments, *Earth planet. Sci. Lett.*, **86,** 389–400.

Zhou, L.P., Oldfield, F., Wintle, A.G., Robinson, S.G. & Wang, J.T., 1990. Partly pedogenic origin of magnetic variations in Chinese loess, *Nature*, **346,** 737–739.

Downloaded from https://academic.oup.com/gji/article/117/1/257/616632 by guest on 16 August 2022